Journal of Nuclear Materials 389 (2009) 213–220

Contents lists available at ScienceDirect

Journal of Nuclear Materials

journal homepage: www.elsevier.com/locate/jnucmat

High temperature surface effects of He^+ implantation in ICF fusion first wall materials

Samuel J. Zenobia *, R.F. Radel, B.B. Cipiti, Gerald L. Kulcinski

Fusion Technology Institute – University of Wisconsin-Madison, 1500 Engineering Drive, Madison, WI 53706, USA

A B S T R A C T

The first wall armor of the inertial confinement fusion reactor chambers must withstand high temperatures and significant radiation damage from target debris and neutrons. The resilience of multiple materials to one component of the target debris has been investigated using energetic (20–40 keV) helium ions generated in the inertial electrostatic confinement device at the University of Wisconsin. The materials studied include: single-crystalline, and polycrystalline tungsten, tungsten-coated tantalum-carbide 'foams', tungsten–rhenium alloy, silicon carbide, carbon–carbon velvet, and tungsten-coated carbon–carbon velvet. Steady-state irradiation temperatures ranged from 750 to 1250 °C with helium fluences between 5×10^{17} and 1×10^{20} He^+/cm^2. The crystalline, rhenium alloyed, carbide foam, and powder metallurgical tungsten specimens each experienced extensive pore formation after He^+ irradiation. Flaking and pore formation occurred on silicon carbide samples. Individual fibers of carbon–carbon velvet specimens sustained erosion and corrugation, in addition to the roughening and rupturing of tungsten coatings after helium ion implantation.

1. Introduction

To make either magnetically or inertially confined commercial fusion reactors economically viable, major maintenance procedures and down time must be minimized. Most often, these maintenance requirements are compromised by failure of the in-vessel materials, such as the first wall (FW) armor. In inertial fusion energy devices, the ability of the FW to withstand temperatures near their operational limit and endure significant radiation damage due to ion, neutron, and X-ray fluxes is crucial to their success.

The high average pulsed laser (HAPL) program [1] proposes the design of a laser driven inertial confinement fusion reactor. High intensity laser pulses implode deuterium–tritium (D–T) pellets at a rep-rate of ~10 Hz. The reference HAPL chamber design is spherical with a radius of 10.5 m. Proposed FW armor coatings are ~1 mm thick and are bonded to the ferritic steel vacuum vessel. One component of the resulting radiation threat spectra is the substantial light ion fluxes ranging in energy from ~10 keV to several MeV which bombard the FW of the HAPL chamber. These ion fluxes thin the armor through sputtering, blistering, and exfoliation. Such events can create radioactive dust which in turn, could degrade laser optics and, if released, could be harmful to the public. Experiments have shown that the high energy portion (>1 MeV) of helium ions results in the blistering of polycrystalline tungsten (a primary first wall candidate) at fluences >10^{17} He^+/cm^2 [2].

The current paper focuses on the low energy portion of this helium ion spectrum (<100 keV) and assesses the resilience of a variety of FW candidate materials to withstand a wide range of He^+ fluences (5×10^{17}–10^{20} He^+/cm^2) while at high temperature (750–1250 °C). In almost every case, this type of irradiation has caused severe damage the material surfaces. The study presented here summarizes ongoing and previous irradiations on several materials, proposes a future direction given the results and presents some important corrections to previous results.

2. Experimental

2.1. The UW-IEC Device

Nominal implantation experiments in the UW inertial electrostatic confinement (IEC) device consist of a tungsten–rhenium mount which holds the irradiated specimen via tension or a spot weld (Fig. 1). This mount is placed inside of a concentric stainless steel anode (diameter = 0.5 m) held at ground potential. The ^4He fuel gas is fed into the vacuum chamber at a pressure of ~0.7 Pa (0.5 mtorr) and ionized via electron bombardment produced by light bulb filaments. Consequently, ^4He ions are attracted to the specimen's (cathode) negative potential and converge normal to the sample resulting in the implantation of the specimen. The ion energy is set by the cathode voltage, from the 200 kV power supply via a high voltage feed thru, and ranges from 20 to 40 kV for the current implantation experiments. This research utilized the UW-IEC device HOMER, whose schematic is shown in Fig. 2.

* Corresponding author. Tel.: +1 608 265 8699; fax: +1 608 263 4499.
E-mail address: zenobia@wisc.edu (S.J. Zenobia).

0022-3115/$ - see front matter © 2009 Elsevier B.V. All rights reserved.
doi:10.1016/j.jnucmat.2009.02.004

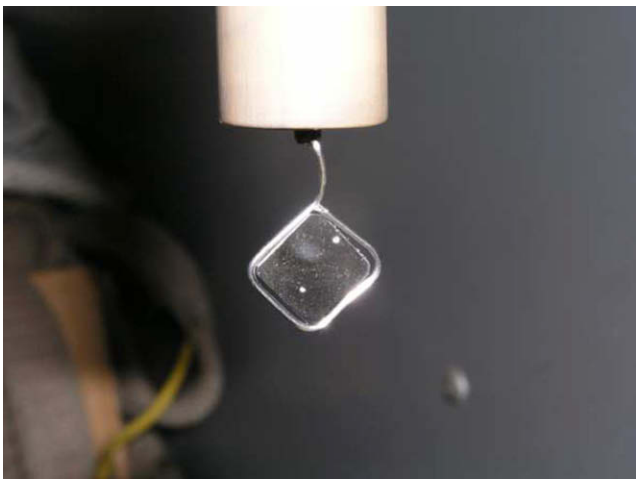

Fig. 1. An unirradiated polycrystalline tungsten sample mounted on the IEC device's HV stalk before implantation [4].

Additional information on HOMER can be found in reference Radel et al. [3].

2.2. Post-irradiation analysis

Scanning electron microscopy images were taken of specimens before and after irradiation. The LEO 1530 field emission scanning electron microscope was used for the majority of imaging, both pre- and post-irradiation. Certain samples were imaged using a Zeiss Crossbeam focused ion beam mill. Elastic recoil detection was performed by on selected specimens to determine helium retention and penetration depth. This was done using the 1.7 MeV Tandem accelerator at UW.

3. Results and discussion

This paper summarizes the previous work of Cipiti which focused on single (SCW) and polycrystalline tungsten (PCW). A summary of Radel's continuation of this work is also presented. Radel also investigated SCW and PCW, but expanded irradiations to include tungsten-coated tantalum-carbide foams (TaC) and tungsten–rhenium alloys (W–Re). The author's work presented in this report will focus on other refractory materials such as silicon carbide (SiC), carbon–carbon velvet (CCV) and tungsten-coated carbon–carbon velvet (W/CCV) materials.

3.1. Single-crystalline tungsten

Early investigations by Cipiti and Kulcinski [4] on PCW, which will be discussed later in this paper, revealed preferential collection of the implanted helium on grain boundaries. This motivated the experimentation with SCW. Using the UW-IEC device HOMER in steady-state mode, Radel and Kulcinski [5] irradiated SCW samples to determine the threshold for surface erosion and pore formation as a comparison to polycrystalline tungsten. Ion doses ranged from 6×10^{17}–10^{19} He^+/cm^2 at irradiation temperatures of ~1100 °C. There has been a temperature correction made to the work previously reported by Radel and Kulcinski [5]. New information on the infrared pyrometer used to measure the sample temperature resulted in a correction to the irradiation temperature from 800 to ~1100 °C for the SCW and W-coated tantalum-carbide foam specimens. It was found that the calibration of the Raytek® Marathon MR pyrometer drifted causing the ~300 °C error. These results revealed that the threshold fluence for significant pore formation was $\sim 3 \times 10^{18}$ He^+/cm^2, though a random distribution of pores were observed as low as 10^{18} He^+/cm^2. At the highest implant fluence of 10^{19} He^+/cm^2, pore formation and surface roughening was extensive. Scanning electron microscopy (SEM) images of these irradiations are shown in Fig. 3.

3.2. Polycrystalline tungsten

Much of ion implantation work done at UW has focused on PCW as it is one of the most attractive FW materials for inertial fusion energy reactor concepts [1]. Experiments done by Cipiti and Kulcinski [4] focused on the steady-state irradiation of PCW specimens and included scans of ion fluence, irradiation temperature, and ion energy. These implantation experiments scanned irradiation temperatures between 800 and 1200 °C. The fluences stated in [4] have been corrected in this paper. Initial values for the PCW specimen's secondary electron emission coefficients where high and yielded fluences of $\sim 10^{16}$–6×10^{17} He^+/cm^2. New information for the secondary emission coefficients of these samples has resulted in a correction to the previously reported fluences

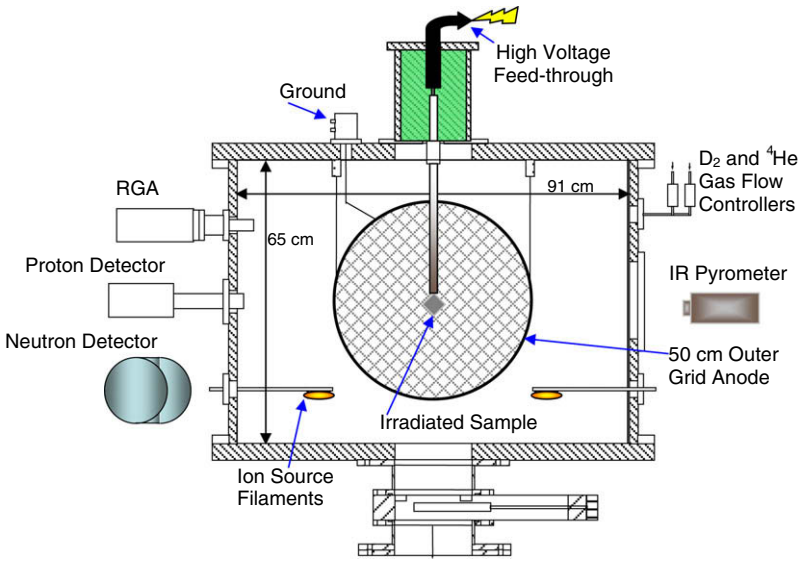

Fig. 2. Schematic of UW-IEC device HOMER.

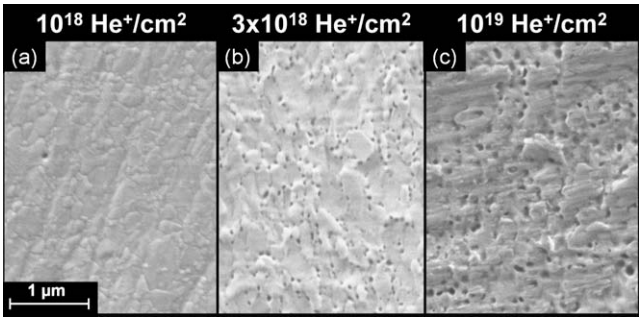

Fig. 3. Single-crystalline tungsten irradiated at ~1100 °C to fluences of (a) 10^{18} (b) 3×10^{18} and (c) 10^{19} He^+/cm^2 [5,6].

and now range from ~10^{17}–10^{19} He^+/cm^2. At 1100 °C the onset of pore formation in PCW occurred at ~10^{17} He^+/cm^2, but became extensive as fluences increased from 10^{18} to 10^{19} He^+/cm^2 (Fig. 4).

The aforementioned irradiations which varied the implantation temperature and ion energy were all performed at a fluence of ~5×10^{18} He^+/cm^2, well above the damage threshold (~10^{17} He^+/cm^2) for PCW. Very few quantitative conclusions were able to be drawn from these temperature and ion energy scans, due to extensive pore formation at these high doses.

Radel et al. expanded on this work by reproducing several of Cipiti's steady-state irradiation results [6] and performing corresponding irradiations in HOMER's pulsed mode to better simulate a pulsed inertial fusion energy reactor [7]. Post-irradiation analyses experiments were also expanded to use a Zeiss Crossbeam focused ion beam mill and electron recoil detection to determine ion penetration depth and helium retention as a function of depth in PCW, respectively. Steady-state irradiations at 1150 °C confirmed the previous results for damage thresholds. Analysis done using elastic recoil detection showed the percentage of ^4He in the PCW specimen's surface saturates at 40 at.%. This occurs at a depth of ~50 nm into the sample's surface (Fig. 5). Furthermore, it was observed that the maximum retained helium fluence in PCW saturated at ~1.2×10^{13} He atoms/cm^3; independent of the implanted fluence.

Pulsed experiments were also performed on PCW specimens at fluences of 10^{18}–10^{19} He^+/cm^2 and irradiation temperatures of 1170 °C. In each case the specimen irradiated in a pulsed environment sustained much more extensive damage to the surface than those irradiated in steady-state conditions. Radel and Kulcinski [7] showed that the pore density for each of the pulsed specimens appeared to saturate. Furthermore, the pore density in the pulsed specimens exceeded the maximum pore density observed in the steady-state samples of 4×10^9 pores/cm^2. An extended sub-surface semi-porous layer was also observed in the pulsed specimens (Fig. 6). At corresponding fluences (10^{18} and 10^{19} cm^{-2}), the depth of this semi-porous layer extended ~2–3 times deeper in pulsed

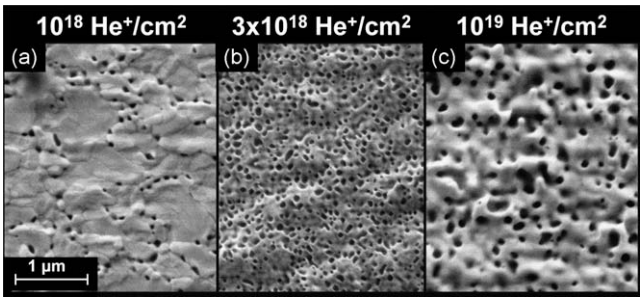

Fig. 4. PCW irradiated at ~1100 °C to fluences of (a) 10^{18} (b) 3×10^{18} and (c) 10^{19} He^+/cm^2 [6].

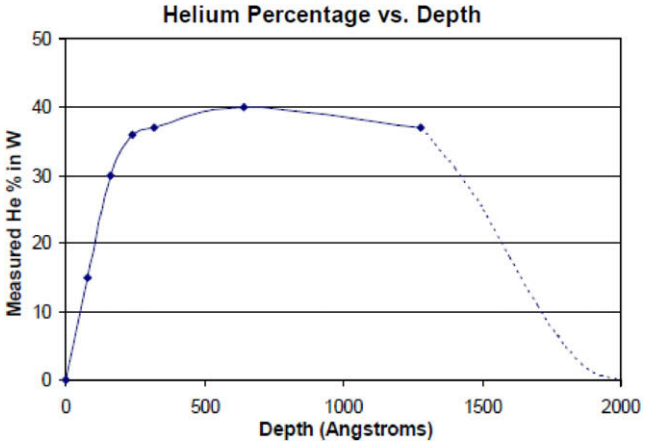

Fig. 5. Depth profile of helium concentration in a polycrystalline tungsten sample irradiated at 1150 °C to 10^{19} He^+/cm^2 [3,6].

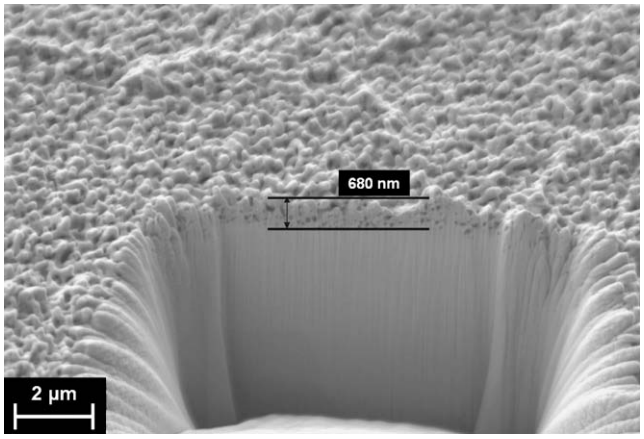

Fig. 6. Polycrystalline tungsten irradiated to 10^{19} He^+/cm^2 at 1150 °C in pulsed mode of the IEC (1 ms pulse width, 25 Hz duty cycle) [7].

samples (300–700 nm) than in those irradiated in steady-state mode (90–300 nm). In every case, the penetration of this semi-porous layer extended beyond the theoretical range of 30–40 keV He^+. SRIM calculations predict an ion range in tungsten of ~60 nm at room temperature. A comparison of surface damage effects is given in Fig. 7 for SCW, steady-state PCW, and pulsed PCW at a constant fluence of 10^{19} He^+/cm^2.

Irradiations on a W–Re alloy (25% Re) were performed by Radel and Kulcinski [6] concurrently with the investigations on pure tungsten. The HAPL program was inspired to do this because of

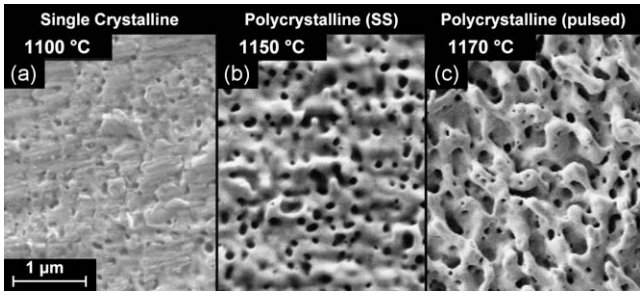

Fig. 7. Comparison of steady-state irradiated single-crystalline (a) and polycrystalline tungsten (b) and pulsed implanted polycrystalline tungsten (c) all at a fluence of 10^{19} He^+/cm^2 [5–7].

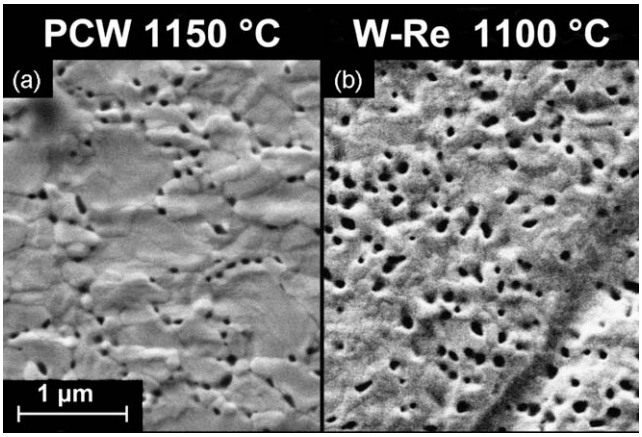

Fig. 8. Comparison of polycrystalline tungsten (a) and W–Re alloy (b) irradiated to 10^{18} He^+/cm^2 [3,6].

the improved mechanical properties of W–Re alloys despite its lower melting point [8]. Steady-state irradiations were performed at fluences between 6×10^{17}–10^{19} He^+/cm^2 at 1100 °C. Fig. 8 compares the pure polycrystalline tungsten to the W–Re alloy at a fluence of 10^{18} He^+/cm^2. While both samples have reached the threshold fluence for pore formation, the W–Re sample already shows a uniform pore distribution across the surface. Conversely, the pure PCW shows the onset of surface morphology change – preferential collection of helium bubbles on grain boundaries. This illustrates a potential decreased damage threshold of W–Re from that of PCW. Another behavior characteristic of the W–Re alloy was an increased average pore diameter from that of the PCW on each of the examined irradiated specimens.

3.3. W-coated tantalum-carbide foams

As a response to the poor performance of the PCW and W–Re alloy after helium ion bombardment, Radel investigated various W-coated TaC foams [5]. These specimens include a large, medium, and fine grain W-coating. Both the medium and fine grain coatings were considered high emissivity or 'high ε' samples due to the addition of fine grain tungsten dendrites. Fig. 9 shows a TaC foam with the W-coating prior to irradiation. It is observed that the coating is very thick (~40 μm) compared to the range of the 30 keV He^+ (~100 nm).

Each of the three types of W-coated TaC foam samples was vacuum annealed at 1200 °C for 30 min to differentiate between thermal effects and ion damage. Annealing resulted in minor roughening of the foam surfaces, but no pore formation. Irradiations were performed on each of the foam grains sizes to a fluence of 10^{19} He^+/cm^2 at ~1100 °C. SEM analysis revealed that all three

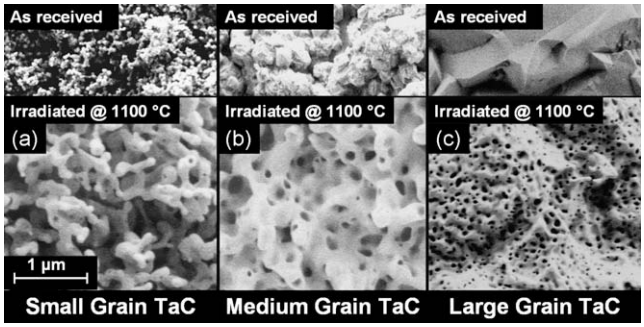

Fig. 10. Comparison of (a) small (b) medium and (c) large grain W-coated TaC foams irradiated at 1100 °C to 10^{19} He^+/cm^2 [5].

samples incurred substantial changes in surface morphology after irradiation (Fig. 10). The implantation caused extensive pore formation on both large and medium grained specimens. Pores are smaller and more numerous on the large grain sample, while the medium grain sample has fewer pores with greater average diameters. It also appears that the dendrites on the medium grain sample have begun to swell and resemble the 'coral-like' surface observed on the pulsed PCW (Figs. 6 and 7). Sizeable swelling of the tungsten dendrites is observed in the fine grain specimen, but pore density is greatly reduced from the large and medium grain samples. The existence or creation (from ion damage) of dendrites on W surfaces is undesirable for the HAPL program, as they may break off easily and produce more radioactive dust or even serve as crack propagation sites. In general, the TaC foams trade pore formation for an apparent growth in dendrite size as the grain size is decreased.

3.4. Tungsten materials summary and comparison

Fig. 11 gives a final comparison of the tungsten materials investigated by Cipiti and Radel. Each of the specimens in Fig. 11 was irradiated in steady-state mode to 10^{19} He^+/cm^2 at a temperature between ~1100 and 1150 °C. These SEM micrographs reveal that the SCW responded the most favorably to irradiation conditions and had a low pore density relative to the other samples. The W–Re alloy incurred the worst damage from irradiation, sustaining a saturated pore density and larger average pore diameters than any other specimen. While pore formation in the PCW sample is extensive, pore density has not saturated and the 'coral-like' microstructure is not dominant as in pulsed irradiations (Fig. 6). W-coated TaC foams sustained increasing pore formation and decreased swelling with increased grain size. Overall, the SCW showed superior resilience to the high temperature ion implantation (>10^{18} He^+/cm^2) followed by the PCW, large grain W-coated TaC, and W–Re alloy in order of reduced resistance to radiation

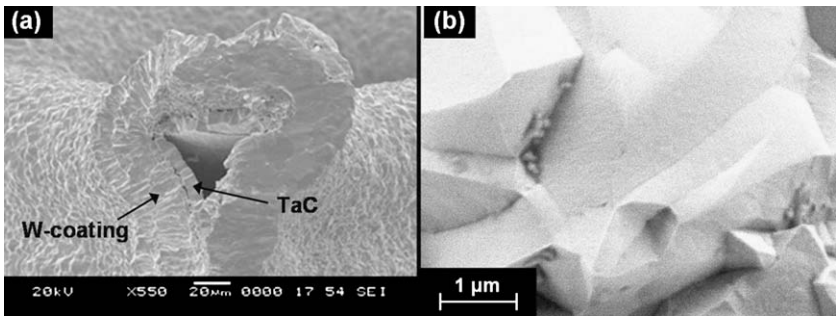

Fig. 9. (a) Cross-section of unirradiated W-coated TaC foam (large grain) and (b) high magnification micrograph of W-coated TaC foam surface prior to irradiation [5].

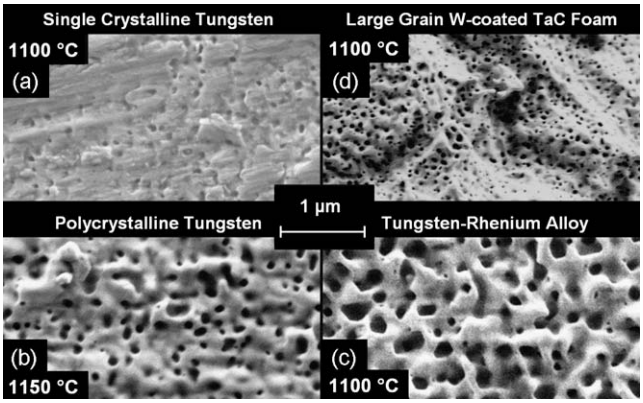

Fig. 11. Comparison of (a) SCW (b) PCW (c) W–Re alloy and (d) large grain W-coated TaC foam irradiated to 10^{19} He^+/cm^2 [5–7].

damage. Unfortunately, SCW is unusable in a first wall application such as the HAPL reference chamber, which calls for a 10.5 m radius vacuum vessel. Such a design would be virtually impossible to implement, given current technology and manufacturing capabilities.

A common thread of helium bubble formation is seen in all of these materials, though the extent differs quantitatively. This is not a new phenomenon as pores or 'pinholes' were seen in vanadium by Thomas and Bauer [9] as early as 1974. Recent theoretical work has been done to assess the formation, migration, and coalescence of these bubbles in a tungsten FW of the HAPL reactor as a result of He^+ implantation [10,11]. Several authors [2,12] have suggested that applying the principle of small or 'micro' grains to PCW might result in a suitable FW material. Unfortunately, this research does not indicate that a micro-grain structure will stop or prohibit the clustering of helium atoms, bubble formation, or bubble coalescence resulting in surface exfoliation.

3.5. Silicon carbide

Despite their brittleness and large scale fabrication difficulties, SiC and graphite, are desirable materials for high temperature nuclear reactors, such as the HAPL program. This is due to their low induced radioactivity, low cost, availability, and high temperature strength [13]. Chemical vapor deposition (CVD) SiC samples were irradiated to fluences of 10^{18} and 10^{19} He^+/cm^2 at three different temperatures (750, 850, and 950 °C) to determine He^+ implantation effects as a function of fluence and temperature. Samples irradiated at 750 °C exhibited substantial surface erosion and morphology changes. The sample irradiated to 10^{18} He^+/cm^2 (Fig. 12(a)) sustained substantial flaking but no noticeable pores, while the high fluence sample (Fig. 13(a)) exhibited larger 'craters'.

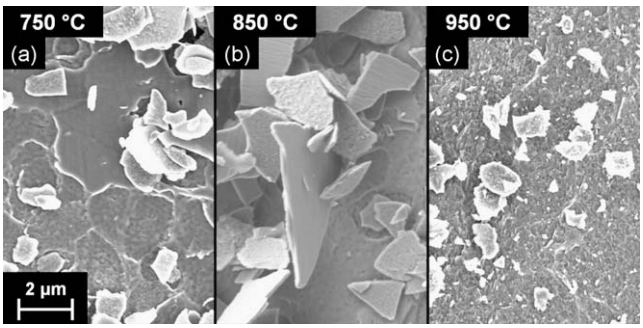

Fig. 12. CVD SiC irradiated to 10^{18} He^+/cm^2 at (a) 750 (b) 850 and (c) 950 °C [14].

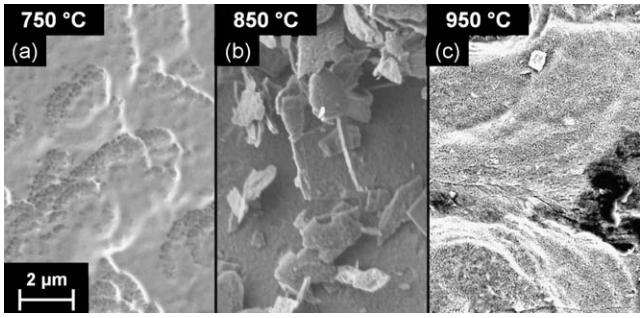

Fig. 13. CVD SiC irradiated to 10^{19} He^+/cm^2 at (a) 750 (b) 850 and (c) 950 °C [14].

These craters were presumably caused by flaking, though no flakes were observed during post-irradiation analysis on the higher fluence sample.

An increased cratering and flaking effect was observed, as well as pore formation, at both implantation fluences at 850 °C. This extensive flaking can be observed at 10^{18} He^+/cm^2 (Fig. 12(b)) and 10^{19} He^+/cm^2 (Fig. 13(b)). Another important observation is the thickness of the flakes on the samples irradiated at 850 °C. Their average thickness is several tenths of a micron, and very near to the range of helium in SiC as calculated by SRIM (Fig. 14). This suggests that repeated flaking might be occurring from gradual erosion, as material redeposits on the SiC surface. Flaking of SiC blisters and their redeposition from He^+ bombardment has also been observed by Yamauchi et al. [14].

Increasing irradiation temperature to 950 °C, resulted in pore formation as well as flaking. In fact, at 10^{19} He^+/cm^2 pore formation seems to dominate the damage, taking on a 'pumice-like' appearance. The large layered depressions are regions that have preferentially flaked away during irradiation. SEM observation showed that crater size and depth increases with temperature. At 950 °C the craters have become large depressions in the surface spanning tens of microns. CVD SiC samples also exhibited inhomogeneous surface damage. Large flake redeposition regions called 'lakes' were seen near the center SiC specimen irradiated to 10^{18} He^+/cm^2 at 850 °C.

The nature of the surface morphology changes incurred in initial CVD SiC irradiation experiments required the verification that ion fluence, not high temperature were causing effects. An experiment was devised which involved masking half of a CVD SiC sample with a tantalum foil. The sample was irradiated to a fluence $\sim 1.1 \times 10^{19}$ He^+/cm^2 at 950 °C over the course of 2½ h. The results of the experiment are presented in Fig. 15. After comparing the portions of the sample which are shielded and unshielded, it is clear that the ion fluence initiates the damage seen on the surface

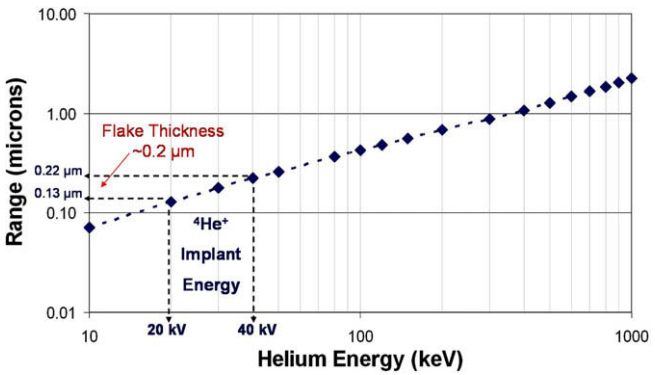

Fig. 14. Range of He^+ in CVD SiC as a function of energy, with IEC implantation energies highlighted [14].

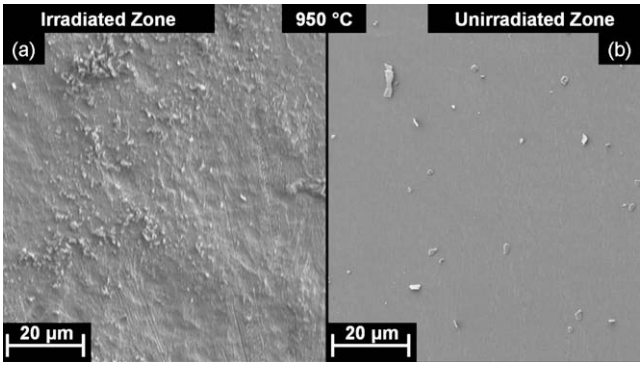

Fig. 15. Irradiated (a) and unirradiated (b) regions of CVD SiC irradiated at 950 °C to 1.1×10^{19} He^+/cm^2 [14].

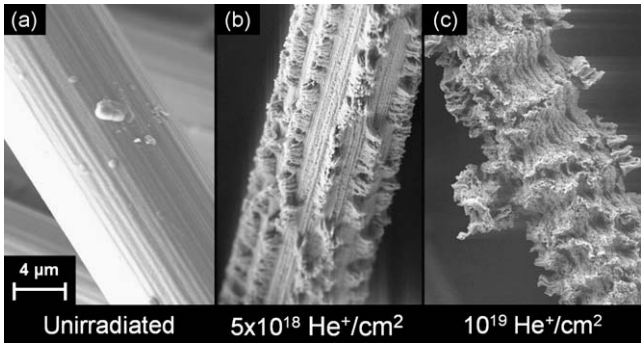

Fig. 17. Unirradiated CCV (a) and CCV implanted to (b) 5×10^{18} and (c) 10^{19} He^+/cm^2 at 1150 °C.

of the CVD SiC samples, not the temperature. Because the tantalum mask was not completely flush against the SiC, the contaminants seen in the unirradiated zone are most likely a result of SiC flakes falling between the tantalum mask and the sample surface. An approximate depth of the surface craters induced by the He^+ was obtained by tilting the masked sample in the SEM stage at 35° and taking micrographs. Results show one of the depressed regions exceeded several microns (~3.2 μm), where it is assumed that repeated flaking occurred. A more detailed presentation of SiC response to He^+ implantation can be found in [15], along with the implications of this response to the HAPL chamber.

3.6. Carbon–carbon velvet

The final focus of this paper is helium implantation in carbon–carbon velvet and W-coated carbon–carbon velvet specimens. This recently developed material is a new candidate for the first wall armor of the HAPL chamber. The motivation behind using CCV and W/CCV as armor materials is to increase the effective surface area of the FW without increasing the radius of the vacuum vessel. For a given operation time, increased surface area decreases the effective fluence and heat flux to the FW materials. Samples are cylindrical in shape with a 4 mm height (including fibers) and 10 mm diameter. Fiber dimensions are ~1 mm long and ~10 μm in diameter. The core material of the fibers is pitch graphitic carbon approximately 9 μm in diameter. These fibers are then CVD coated by an amorphous carbon layer (~0.5 μm). To complete W/CCV samples an additional sputter coating of tungsten ~1 μm thickness is applied. This process is illustrated in Fig. 16.

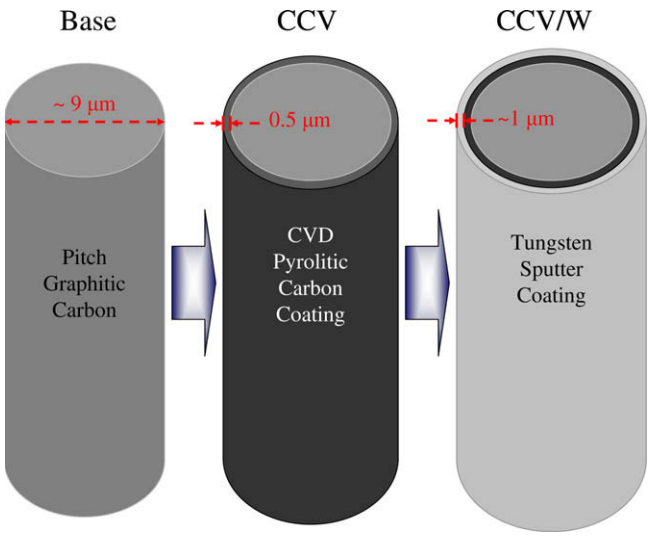

Fig. 16. Schematic of fabrication process for CCV and W/CCV fibers.

Steady state helium ion implantation of a CCV samples was performed at 1150 °C to a fluences of 5×10^{18} and 10^{19} He^+/cm^2. Fig. 17 compares the virgin CCV to the irradiated specimen. At 5×10^{18} He^+/cm^2 the CCV's outer pyrolitic coating of carbon is almost completely eroded away, leaving the inner pitch graphite substrate exposed. Helium ions only have a range of ~0.2 μm in amorphous carbon which is appreciably shorter than the ~0.5 μm coating on the fiber shafts. Most likely, this occurs due to a gradual erosion of the amorphous layer during the He^+ implantation process, eventually exposing the core of the fiber shaft. Once vulnerable, the helium ions attack the graphine planes causing their separation and expansion. The results of exposing this pitch graphite can be seen at 10^{19} He^+/cm^2 (Fig. 17(c)). A final result is the severe exfoliation of the fiber tips and fiber shaft corrugation. Furthermore, graphitization of the carbon fibers comprising these velvet specimens is not believed to occur during irradiation at 1150 °C as these carbon fibers have been annealed to 3000 °C by the vendor [16]. In each of the irradiations performed on the CCV specimens, significant morphology change is evident.

It is inferred that the threshold fluence of these specimen is much lower than the minimum tested fluence of 5×10^{18} He^+/cm^2. Similar experiments were performed by Ekern et al. [17] on graphite cloth and showed flaking of the graphite surface after He^+ implantation. It should be noted that his experiments were performed between room temperature and 800 °C and showed a decrease in damage with increasing temperature. Moreover, the type of graphite composing the velvet fibers might play a large role in either reducing or enhancing radiation damage. Thomas [18] observed cracking perpendicular to the surface in edge orientated graphite as opposed to flaking in basal orientate graphite after bombardment with 300 keV He^+. It is quite possible that a pan (stacked graphine planes) fiber might respond more favorably to ion implantation.

3.7. Tungsten-coated carbon–carbon velvet He^+ irradiation

The second type of velvet sample investigated was the W/CCV irradiated at ~1150 °C to a fluence of 5×10^{18} and 10^{19} He^+/cm^2. SEM micrographs in Fig. 18(a) illustrate the unirradiated W/CCV. Fig. 18 reveals that the helium implantation caused surface roughening and pore formation over the entire tip and shafts of the fibers at both fluences. Unlike CCV samples, tip erosion is not observed, but the tungsten sputter coating has ruptured along shafts and on the tips of various fibers. Once ruptured, fiber shafts and tips undergo the same tip exfoliation and fiber shaft corrugation seen in the He^+ implanted CCV specimen.

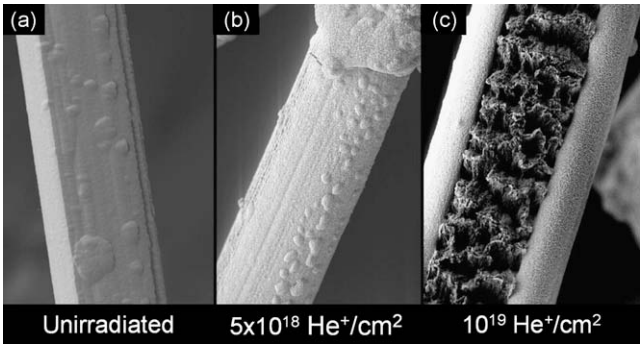

Fig. 18. Unirradiated W/CCV (a) and W/CCV implanted to (b) 5×10^{18} and (c) 10^{19} He^+/cm^2 at 1150 °C.

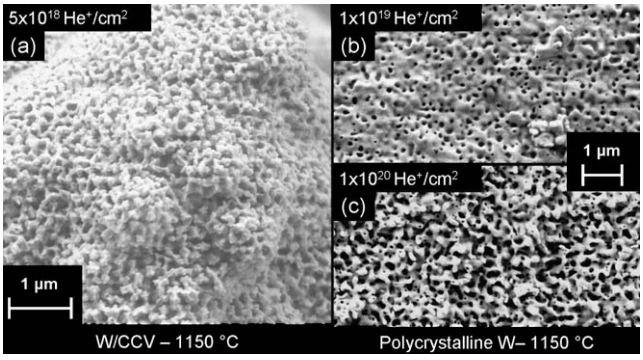

Fig. 19. Comparison of W/CCV irradiated to (a) 5×10^{18} He^+/cm^2 at 1150 °C and PCW irradiated to (b) 10^{19} and (c) 10^{20} He^+/cm^2 at 1150 °C [6].

Rupturing of the tungsten coatings are caused by the different thermal expansion coefficients between tungsten (4.9×10^{-6} m/m K) and the graphitic carbon (8×10^{-6} m/m K). The coefficients listed above are average values, but in pitch carbon will shrink vertically and expand radially under heat. The expansion coefficient for radial expansion of graphite is 27×10^{-6} m/m K and the vertical expansion coefficient is -1.5×10^{-6} m/m K. Using the values of the average expansion coefficients, for a 10 μm diameter fiber at ~1150 °C the tungsten coating will expand ~55 nm radially, while the carbon will expand ~90 nm radially. This difference causes stress and is possibly the cause of the observed rupturing. A final observation of the W/CCV fiber tips (5×10^{18} He^+/cm^2, 1150 °C) at increased magnification shows pore formation similar to that of polycrystalline tungsten irradiated to 10^{19} and 10^{20} He^+/cm at 1100 °C (Fig. 19). This micrograph shows that, in the best case scenario, W/CCV responds to He^+ implantation in the same way as the PCW. In addition to pore formation fiber shafts often undergo rupturing at high temperature exposure, causing premature failure of the coating. After rupturing and exposure of the graphite, fibers sustain the same extensive damage as the uncoated CCV.

3.8. Summary

Fig. 20 summarizes the results of all of the materials irradiation experiments performed in the University of Wisconsin IEC apparatus. The plotted lines of the figure each represent the author's best estimate of a material's response to He^+ implantation. Regions to the right of the curves indicate what temperatures and fluences the materials would be not viable for application in a reference HAPL chamber design. Material viabilities were only assessed by surface morphology change in response to irradiation and were quantified by surface erosion, pore density, and specimen mass loss. Future research to investigate the strengths and weaknesses of these and other materials should be pursued. Once the mechanism of helium ion damage is more properly understood, more intelligent FW materials can be developed.

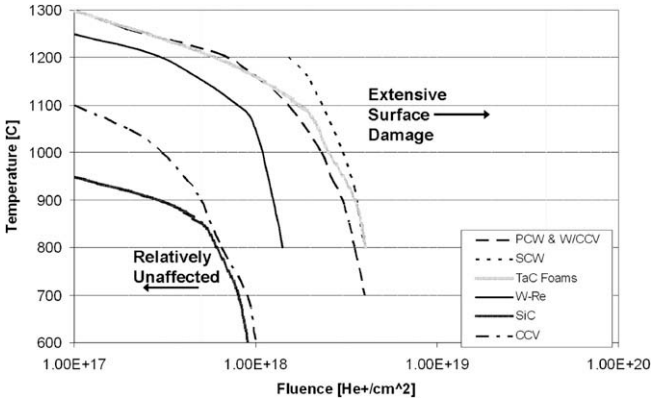

Fig. 20. Materials summary showing regions of viability and non-viability as a function of fluence and implantation temperature.

4. Conclusions

Conclusions are drawn for each of the investigated materials from the data presented above.

SCW exhibits a higher threshold fluence for pore formation than PCW. Additionally, at higher fluences the average pore density of SCW is lower than that of PCW specimens.

Steady-state irradiation of PCW revealed the onset of pore formation at ~10^{17} He^+/cm^2, becoming extensive at fluences >10^{18} He^+/cm^2. The concentration of helium atoms in the surface layer of PCW saturates at ~40 at.%.

Pulsed implantation experiments on PCW resulted in an apparent saturation of pore density at all fluences. Furthermore, at a fluence of 10^{19} He^+/cm^2 the semi-porous layer extended up to 700 nm into the surface after pulsed bombardment with 40 keV $^4He^+$, while this layer depth in steady-state implantations of 30 keV $^4He^+$ extended only 300 nm.

Vacuum annealing of W-coated carbide foams caused minor surface roughening. Large and medium grain carbide foams experienced extensive pore formation similar to that of PCW. The small grain carbide foam showed a reduction in pore density, but substantial swelling of the tungsten dendrites comprising the surface.

Tungsten–rhenium alloys showed a larger average pore diameter than PCW, as well as a lower threshold fluence for pore formation.

A partially masked CVD SiC sample verified that ion flux, not high temperature exposure, causes the observed surface modification of SiC.

CVD SiC has responded very poorly to He^+ irradiation in the parameter space studied in this work. Light ions easily penetrate the material, flaking and exfoliation of the SiC surface results in severe damage to specimens.

CCV specimens experience severe erosion of the fiber tips and shafts. The pyrolytic carbon coating has been partially or completely eroded away in each of the performed irradiations.

W/CCV sustained extensive pore formation over the tungsten coating surface and appears to respond very similarly to PCW. Irradiation temperatures of 1150 °C cause rupturing of the tungsten coating and exposure of the graphite on the carbon fibers.

References

[1] J.D. Sethian, A.R. Raffray, J. Latkowski, J.P. Blanchard, L. Snead, T.J. Renk, S. Sharafat, J. Nucl. Mater. 347 (2005) 161.
[2] S.B. Gilliam, S.M. Gidcumb, N.R. Parikh, D.G. Forsythe, B.K. Patnaik, J.D. Hunn, L.L. Snead, G.P. Lamaze, J. Nucl. Mater. 347 (3) (2005) 289.
[3] R.F. Radel, G.L. Kulcinksi, R.P. Ashley, J.F. Santarius, G.R. Piefer, D.R. Boris, R. Giar, B. Egle, C. Seyfer, S.J. Zenobia, E. Alderson, Trans. Am. Nucl. Soc. 95 (2006) 12.
[4] B.B. Cipiti, G.L. Kulcinski, J. Nucl. Mater. 347 (2005) 298.
[5] R.F. Radel, G.L. Kulcinski, Fus. Sci. Technol. 47 (4) (2005) 1250.
[6] R.F. Radel, G.L. Kulcinski, J. Nucl. Mater. 367–370 (2007) 434.
[7] R.F. Radel, G.L. Kulcinski, Fus. Sci. Technol. 52 (3) (2006) 544.
[8] Goodfellow Corporation Online Database. W and W–Re Properties, <http://www.goodfellow.com/csp/active/gfHome.csp>.
[9] G.J. Thomas, W. Bauer, J. Nucl. Mater. 53 (1974) 134.
[10] Q. Hu, S. Sharafat, Fus. Sci. Technol. 52 (3) (2006) 574.
[11] A. Takahashi et al., in: Presented at the 15th High Average Power Laser Program Workshop, San Diego, CA, 8 August 2006.
[12] S. Sharafat, N.M. Ghoniem, M. Anderson, B. Williams, J.P. Blanchard, L. Snead, J. Nucl. Mater. 347 (3) (2005) 217.
[13] R.A. Matheny, J.C. Corelli, G.G. Trantina, J. Nucl. Mater. 83 (2) (1979) 313.
[14] Y. Yamauchi, Y. Hirohata, T. Hino, J. Nucl. Mater. 313–316 (2003) 408.
[15] S.J. Zenobia, G.L. Kulcinski, Prepared for 17th ANS Topical on Fusion Energy (TOFE), UWFDM 1339.
[16] T. Knowles, private communication, Energy Science Laboratories Inc., San Diego, CA, 2008.
[17] R. Ekern, S.K. Das, M. Kaminsky. in: IEEE 6. Symposium on Engineering Problems of Fusion Research, San Diego, CA, 17 November 1975.
[18] G.J. Thomas, in: Proceedings of the American Chemical Society Meeting, Chicago, Illinois, 25–26 August 1975.